Liver 2002: 22: 330–341
Printed in Denmark. All rights reserved

Liver
ISSN 0106-9543

In vivo quantification of ageing changes in the rat liver from early juvenile to senescent life

Vollmar B, Pradarutti S, Richter S, Menger MD. *In vivo* quantification of ageing changes in the rat liver from early juvenile to senescent life. Liver 2002: 22: 330–341. © Blackwell Munksgaard, 2002

Abstract: *Aims/Method:* Using high resolution multifluorescence *in vivo* microscopy, the present study was undertaken to determine the changes in rat hepatic tissue architecture and microvasculature during the growth associated with juvenile maturation and adult senescence, i.e. the age of 1, 3, 12 and 24 months. *Results:* By 1 month of age the liver attained its full size and functional capacity, as assessed by relative organ weight and hepatic bile flow. Survey of liver architecture revealed a progressive growth of lobular area with postsinusoidal venules exhibiting a proportional increase in length, diameter and inter-vascular distance up to the age of 12–24 months. In regard to the 3.5–4-fold average increase of lobular units, a minor reduction of sinusoidal density to 87% over life strongly implies the recruitment or formation of new sinusoidal microvessels as contributing mechanism to meet oxygen demand due to overall tissue enlargement. The sinusoidal perfusion rate remained above 98% over the whole lifespan. Leukocytic interaction with the hepatic microvascular endothelium was found within the physiological range in all age groups. Moreover, kinetics of clearance of latex beads as well as lobular distribution of Kupffer cells did not differ between animals of different age. Hepatic stellate cell-associated area of ultraviolet vitamin A-autofluorescence increased with age and significantly correlated with increasing tissue concentrations of vitamin A metabolites. Biochemical parameters serving as measures of tissue integrity did not indicate age-associated tissue alterations. *Conclusion:* These age-associated physiological changes should be carefully taken into account as a relevant variable in experimental research.

Brigitte Vollmar, Sascha Pradarutti, Sven Richter and Michael D. Menger

Institute for Clinical & Experimental Surgery, University of Saarland, 66421 Homburg/Saar, Germany

Key words: ageing – hepatic microcirculation – intravital fluorescence microscopy – Ito cell – Kupffer cell

Brigitte Vollmar, MD, Institute for Clinical and Experimental Surgery, University of Saarland, 66421 Homburg/Saar, Germany.
Tel: 49 6841 16 26554.
Fax: 49 6841 16 26553.
e-mail: exbvol@med-rz.uni-sb.de

Received 4 July 2001,
accepted 11 February 2002

Maturation and ageing to adulthood and senescence are characterized by adaptive processes of vital organs to meet changing demands. Knowledge about the influence of ageing on physiology of vital organs including the liver is important for a better understanding of the ability of an organism to respond to environmental stress as well as various exogenous and endogenous stimuli. So far, most of the studies are restricted to the age-related change in metabolic activities of liver enzymes in terms of activation or detoxification of hepatotoxic compounds (1–3), indicating that old patients are more sensitive to the action of some hepatotoxins than younger ones. Although it is well accepted that the hepatic clearance of many drugs is reduced in the elderly, the precise mechanism of such age-dependent decline in organism resistance is still largely unclear. While a decreased microsomal drug metabolism is considered to be a reason for prolonged action and increased rate of side effects on old age (4), there are also reports on unchanged activities and substrate affinity of several drug metabolizing enzymes in humans with advancing age (5, 6). An important contribution to the reduced hepatic elimination is also thought to be due to the reduction in liver size and the fall in blood flow, as observed in elderly subjects (6, 7). In addition, some studies have centred on cellular and humoyral factors contributing to age-associated differences in sensitivity of the liver to toxicants (8–10). In this context, it has been speculated

that age-differing properties of Kupffer cells and neutrophils are responsible for the increase of severity of hepatotoxicity observed in aged animals (10–12).

Surprisingly, it is not clear to which extent age-inherent differences in microangioarchitecture, cellularity, microvascular haemodynamics and nutritive tissue perfusion of the liver exist and whether they are contributing factors of age-related susceptibility of the liver. As the individual organs enlarge during maturation, the microcirculation must provide for the nutritional needs of changing tissue mass. Thereby, growth of new vessels or elongation of existing vessels can occur as microvascular mechanisms contributing to organ growth, similarly as vessel regression and involution might appear as an adaptive response of the organ to reduced metabolism at advanced age. On reviewing the relevant literature in the field of maturation and ageing, however, one recognizes that the liver microcirculation has somehow escaped attention. To address this lack of information, the current study was undertaken to more clearly define the changes in hepatic microvascular morphology and cellularity as well as hepatic microhaemodynamics during the development from neonate and early juvenile to adult and senescent.

Materials and methods

Animal model

Male Sprague–Dawley rats at the age of 1 month ($n = 6$), 3 months ($n = 6$), 12 months ($n = 6$) and 24 months ($n = 6$) were used for the experiments. Given that the natural life cycle of Sprague–Dawley rats is approximately 30 months (13), animals at the age of 3 months and 12 months can be considered as young and mature, while 24 month-old-animals are to be seen as senescent individuals. One month-old-animals are weaning rats. Animals were kept on water and standard laboratory chow *ad libitum*. The experiments were conducted in accordance with the German legislation on protection of animals and the *NIH Guide for the Care and Use of Laboratory Animals* (Institute of Laboratory Animal Resources, National Research Council). Under pentobarbital anaesthesia (50 mg/kg body weight ip) the animals were tracheotomized to facilitate spontaneous respiration (room air) and placed in supine position on a heating pad for maintenance of body temperature at 36–37 °C. Polyethylene catheters (PE 50, ID 0.58 mm, Fa. Portex, Hythe, UK) in the right carotid artery and jugular vein allowed for the assessment of systemic haemodynamics, injection of fluorescent dyes for intra-vital microscopy and permanent infusion of isotonic saline solution at a rate of 2 mL/kg body weight × h. Following transverse laparotomy and cannulation of the common bile duct (PE-50) for continuous collection of bile, the animals were positioned on their left side. The left liver lobe was then exteriorized and covered with a glass slide for intra-vital fluorescence microscopy (14).

Intravital fluorescence microscopy

Using a modified fluorescence microscope with a 100 W HBO mercury lamp (Axiotech, Zeiss, Jena, Germany), attached to a blue filter system (450–490 nm/ > 520 nanometer by, excitation/emission wavelength), the hepatic microcirculation was analysed in epi-illumination. The microscopic images were recorded by a CCD video camera (FK 6990, COHU, Prospective Measurements Inc., San Diego, CA, USA) and transferred to a video system (S-VHS Panasonic AG 7350, Matsushita, Tokyo, Japan). Using a water immersion objective (W 20x/0.5; Zeiss, Jena, Germany) magnification of × 730 was achieved on the video screen (PVM-2130 QM, Sony, Munich, Germany).

Contrast enhancement was achieved by blue light epi-illumination after iv injection of sodium fluorescein (2µmol/kg iv; Merck, Darmstadt, Germany) and allowed for planimetric determination of morphologic parameters and analysis of sinusoidal perfusion (14). The use of a green filter system (530–560 nm/ > 580 nm) allowed for assessment of leucocyte–endothelial cell interaction after staining the leucocytes *in vivo* by intravenous injection of rhodamine-6G (2µmol/kg iv; Merck, Darmstadt, Germany) (15). For intravital microscopic analysis of number and phagocytic activity of KC, plain fluorescent latex particles (diameter 1.1µm; Polyscience Inc., Warrington, PA) were injected intra-arterially through the carotid catheter (3.10^8/kg in 1 mL isotonic saline) (16, 17).

Quantitative video analysis

Quantitative assessment of hepatic morphology and microcirculation was performed off-line by frame-to-frame analysis of the videotaped images using a computer-assisted image analysis system (CapImage; Zeintl, Heidelberg, FRG) (18). Determination of morphologic parameters included the planimetric assessment of the individual lobular size (mm^2), the length (µm), diameter (µm) and intravascular space (μm^2) of postsinusoidal venules as well as the distance between postsinusoidal venules (venulo-venular distance, µm). Length of postsinusoidal venules was assessed by drawing a straight line from the point where more than three sinusoids converged, finally forming

the venule to the central point where the venule disappeared into the depth of liver tissue. Within 10 lobules per animal, sinusoidal perfusion failure was determined by counting the number of non-perfused sinusoids (given in percentage of all sinusoids visible) (14). Sinusoidal density was determined by counting the number of midzonal sinusoids crossing a 200-μm raster line (19). Within 10 lobules per animal, diameter (D) and blood flow velocity were assessed in five midzonal sinusoids per lobule. Volumetric blood flow in each individual sinusoid (Q_s) was calculated from the cross sectional area ($\pi * (D/2)^2$) and blood flow velocity (V) according to the equation of Gross and Aroesty (20): $Q_s = \pi * (D/2)^2 * V$. Thus, volumetric blood flow was analysed in a total of 50 individual sinusoids per animal per experimental group of age.

Leukocyte–endothelial cell interactions were was analysed within 10 hepatic lobules and 10 post-sinusoidal venules per animal, including (i) the number of stagnant leucocytes, located within sinusoids (given as cells/lobule), and not moving during an observation period of 20 s (ii) the number of rolling leucocytes (given in percentage of non-adherent leucocytes), moving within post-sinusoidal venules at a velocity less than two-fifths of the centreline velocity, as well as (iii) the number of adherent leucocytes, located within post-sinusoidal venules (given as cells/mm^2 endothelial surface, calculated from diameter and length of the vessel segment studied, assuming cylindrical geometry), and not moving or detaching from the endothelial lining during an observation period of 20 s (15). Sinusoidal and venular leucocyte flux (cells/min) represent all free-flowing cells passing the individual microvascular segment within one minute.

Spatial distribution of sites of hepatic stellate cell-associated vitamin A autofluorescence was assessed by densitometric recording of positive sites of fluorescence per single frame (75×75 μm) within the individual periportal, midzonal and pericentral zones of liver lobules (21). The area of positive vitamin A sites was calculated automatically as percent of the whole area of the single frame. Kinetics of vitamin A photobleaching served as indirect parameter of hepatic stellate cell-associated vitamin A content.

Phagocytic activity of KC was assessed by the determination of the kinetics of latex particle adherence off-line by frame-to-frame analysis of the videotaped images. Distribution of latex particles adherent in periportal, midzonal and pericentral segments of the sinusoids was expressed as the percentage of all particles visible within the lobule. For assessment of kinetics of particle adherence, 10–15 observation fields per animal were analysed successively within 5 min after injection. The kinetics of adherence was quantified by determining the number of particles moving in sinusoids as the percentage of all particles visible in the lobules during observation for 10 s (16, 17). Since variations in absolute number of beads per lobule were found in association with alterations of sinusoidal perfusion, all data were normalized and expressed as percent of particles visible in sinusoids per microscopic field.

Sampling and assays

Bile flow was measured continuously over 20 min via the catheter in the common bile duct and standardized per g liver wet weight (μl/g × 20 min). At the end of the experiments, arterial blood samples were taken for standard spectrophotometric determination of serum activities of aspartate aminotransferase (AST), alanine aminotransferase (ALT), glutamate dehydrogenase (GLDH), and alkaline phosphatase (AP), which served as indicators for hepatocellular disintegration (AST, ALT, GLDH) and osteogenesis (AP). Liver tissue sections were sampled and stored at − 70 °C until extraction for the determination of vitamin A metabolites. Moreover, liver tissue specimens were fixed in 4% PBS-buffered formalin for histomorphological examination.

High pressure liquid chromatography (HPLC)

For high pressure liquid chromatographic analysis, liver tissue sections were homogenized in Hank's balanced salt solution and de-proteinised using methanol (v/v) containing 50 μg/mL retinyl acetate as internal standard. After vigorous vortexing, samples were extracted by addition of hexane (1:2.5 v/v) and centrifugation at 18000 g for 2 min. The supernatants were dried under reduced pressure to a waxy consistency (Univapo 100H, Axon, Kaiserslautern, Germany) and resuspended in methanol for final analysis.

Retinol and retinyl esters were determined in 20 μl aliquots by use of a HPLC system (Merck, Darmstadt, Germany) using a Rheodyne® injector (Cotati, CA, USA), a L-6200 A Merck-Hitachi pump, and an analytical LiChroCart column (Merck, LiChrospher 250 × 3mm, RP select B, 5 μm particle size) preset with a LiChrospher 100 RP-18 endcapped guard column. Isocratic elution with a mobile phase of methanol:water (95:5 v/v) at a flow rate of 0.8 mL/min was applied. Absorbance of vitamin A and metabolites was monitored at 325 nm using a Merck-Hitachi detector type L-4000. Data were calculated using the chromatography data station software (Merck D-7000).

To identify the various vitamin A metabolites present in rat liver, retention times of commercially available retinoids, i.e. retinol, retinyl oleate, retinyl plamitate and retinyl stearate (Sigma) were determined. Stock solutions of these retinoids were prepared in ethanol at a concentration of 10 mg/mL and stored in darkness at – 20 °C. As external standards, working solutions of retinoids were prepared at various concentrations (10 – 100 µg/mL) in methanol and served for calculation of retinoid concentrations in rat liver samples. The use of retinyl acetate as internal standard allowed for correction for loss of metabolites during the procedure.

Statistical analysis

All data are expressed as mean ± SEM. After disproving the assumption of normality and equal variance across groups, differences between groups were assessed using the Kruskal–Wallis one-way analysis of variance on ranks (overall differences) followed by the Student-Newman-Keuls method (pairwise multiple comparisons). Correlations between fluorescence microscopically assessed parameters as well as between Ito cell-associated vitamin A autofluorescence and liver tissue retinoid contents were tested using linear regression analysis. Overall statistical significance was set at $p < 0.05$. Statistics were performed using the software package SigmaStat (Jandel Corporation, San Rafael, CA, USA).

Results

Systemic parameters

Mean body weight of the experimental animals, which aged 1, 3, 12 and 24 months, was 128 ± 23 g, 322 ± 17 g, 630 ± 67 g and 512 ± 17 g, respectively (Table 1). In contrast to the 4- to 5-fold increase of body weight, liver weight increased from ~5 g at the age of one month to approximately 14.5 g at the age of 12 and 24 months. Thus, liver-to-body weight ratio was highest at the age of one month with 3.8 ± 0.2%, while it ranged between 2.4 and 2.9% at the age of 3–24 months (Table 1).

Systemic haemodynamic parameters, such as mean arterial blood pressure and heart rate paralleled changes known to occur in man. Heart rate was found to be highest younger animals with mean values of 423 ± 12, 340 ± 25, 314 ± 18 and 234 ± 9 beats/min from neonate young, adult and senescent animals respectively (Fig. 1A). In contrast, blood pressure increased from 94 ± 6 to 120 ± 5, 131 ± 8 and 132 ± 7 mmHg at 1–24 months of age (Fig. 1B). Animals of either age did not differ in regard to arterial blood cell count and haematocrit, as well as arterial blood oxygen saturation, gas parameters and pH (Table 1).

Liver morphology and angioarchitecture

In general, lobular morphology of the liver did not differ between the four groups of age studied inasmuch as the observed liver tissue clearly exhibited the polygonal network of capillary sinusoids with drainage of blood flow into central postsinusoidal venules. While the periportal region could regularly be recognized by the stellate origin of the periportal sinusoids, afferent microvessels, i.e. terminal hepatic arterioles and terminal portal venules could rarely be observed regardless the age of the animal. Postsinusoidal venules running in parallel to the liver surface could regularly be observed in animals of either age. Thus, the classical lobular architecture with a hexagonal structure of parenchyma surrounding the central postsinusoidal venule and bordered by the portal fields at the corners of the hexagon was found maintained over age.

By planimetry, quantitative analysis of the lobular structure of liver parenchyma revealed an average lobular size of 0.188 ± 0.021 mm^2 in livers

Table 1. Body and liver weight, arterial blood leucocyte count, haematocrit, pH and arterial blood gas parameters in rats at the age of 1, 3, 12, and 24 month

	1 month	3 month	12 month	24 month
Body weight (g)	128 ± 23*	322 ± 17#	630 ± 67	512 ± 17
Liver weight (g)	5.0 ± 1.0*	9.4 ± 0.5#	14.5 ± 0.9	14.4 ± 0.7
Liver–body weight ratio	3.8 ± 0.2*	2.9 ± 0.2	2.4 ± 0.2	2.9 ± 0.2
leucocyte count (× 10^3/µl)	5.7 ± 0.6	11.5 ± 0.7	8.4 ± 0.6	7.1 ± 0.6
Hct (%)	44 ± 1	47 ± 2	48 ± 2	48 ± 1
pH	7.29 ± 0.02	7.35 ± 0.02	7.34 ± 0.02	7.37 ± 0.02
SaO_2 (%)	94.4 ± 1.0	96.9 ± 0.2	95.4 ± 0.8	96.8 ± 0.4
PaO_2 (mmHg)	81.8 ± 4.4	95.3 ± 2.7	87.1 ± 5.4	94.8 ± 4.3
$PaCO_2$ (mmHg)	47.6 ± 2.7	46.4 ± 1.8	45.5 ± 4.1	48.0 ± 2.1

Abbreviations: Hct, haematocrit; SaO_2, arterial blood oxygen saturation; PaO_2, arterial blood oxygen partial pressure; $PaCO_2$, arterial blood carbon dioxide partial pressure. All values are given as mean ± SEM, each group $n = 6$. * $P < 0.05$ versus 3, 12 and 24 months; # $P < 0.05$ versus 12 and 24 months.

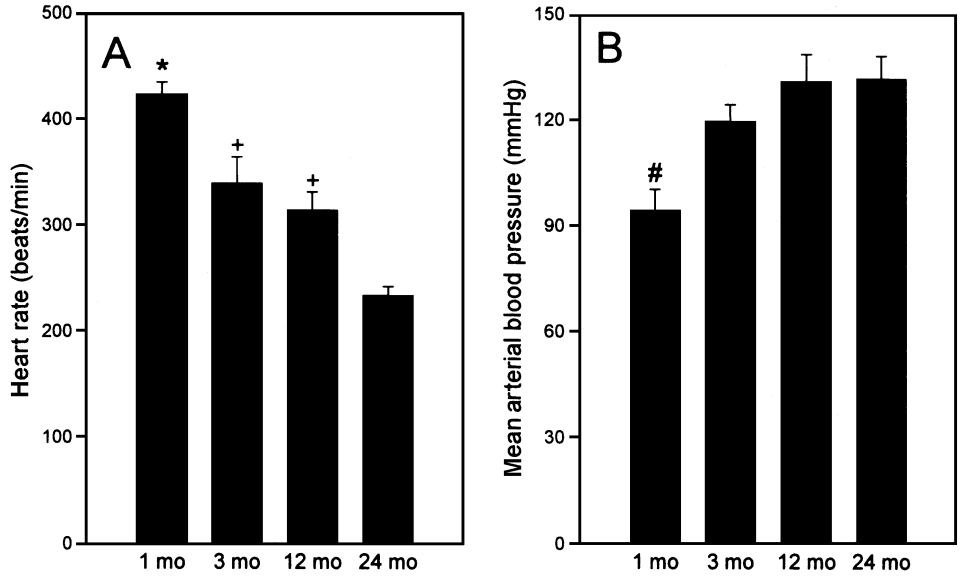

Fig. 1. Heart rate (A) and mean arterial blood pressure (B) in rats at the age of 1 month ($n = 6$), 3 months ($n = 6$), 12 months ($n = 6$) and 24 months ($n = 6$). Mean ± SEM. * $P < 0.05$ versus 3, 12 and 24 months; # $P < 0.05$ versus 12 and 24 months; + $P < 0.05$ versus 24 months.

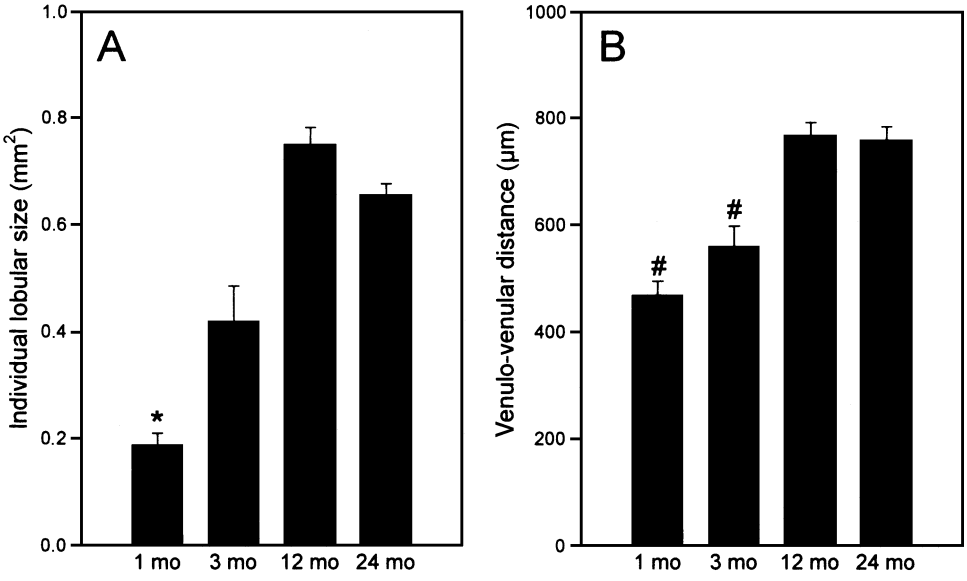

Fig. 2. Size of individual lobules (A) and distance between postsinusoidal venules (B) in livers of rats at the age of 1 month ($n = 6$), 3 months ($n = 6$), 12 months ($n = 6$) and 24 months ($n = 6$). Parameters were assessed by means of *in vivo* fluorescence microscopy and epi-illumination after contrast enhancement by sodium fluorescein. Mean ± SEM. * $P < 0.05$ versus 3, 12 and 24 months; # $P < 0.05$ versus 12 and 24 months.

at the age of one month, which increased to $0.420 \pm 0.066\,mm^2$ and $0.749 \pm 0.033\,mm^2$ up to the age of 3 and 12 months (Fig. 2A). At the age of 24 months, however, lobules barely reached an average size of $0.655 \pm 0.021\,mm^2$ (Fig. 2A). With growth of lobular areas, the individual distance between the central postsinusoidal venules increased proportionally (Figs 2B and 3), as given by the significant correlation ($P = 0.018$, $r^2 = 0.965$). In parallel, postsinusoidal venules increased both in length and diameter (Table 2; Fig. 3). While lobules ceased in growth at 12 month of age, longitudinal and transverse growth of venules was observed up to the age of 24 months (Table 2).

Sinusoidal density, i.e. the number of sinusoids crossing a 200 µm-line, was found to slightly but steadily decrease from neonate to young, adult and senescent life, however, without any evidence for impairment of nutritive perfusion (percentage of non-perfused sinusoids < 2% in all animals of either age) (Table 2).

Sinusoidal blood flow was conserved regardless of age ranging between 7 and 9 pL/ s (Table 2), while weanling one month-old-animals revealed significantly smaller sinusoidal diameters with higher flow velocities when compared to animals of higher age (Table 2).

Intrahepatic cellularity and hepatic tissue vitamin A content

As assessed by HPLC, retinol, retinyl oleate, retinyl palmitate and retinyl stearate content of livers in animals of different age is shown in Table 3. The vitamin A content markedly increased during the lifespan of rats with a ~two-fold increase of retinol, a ~32-fold increase of retinyl stearate, a ~53-fold increase of retinyl palmitate, and a ~66-fold increase of retinyl oleate. Vitamin A was found present in rat liver mainly as the retinyl esters retinyl palmitate and stearate.

Hepatic stellate cells were indirectly assessed by the *in vivo* visualization of the autofluorescence of intracellularily stored vitamin A. By counting punctate fluorescence spots, a progressive decrease of the number of spots was found with increase of age (Figs 4A and 5). However, areas of the individual punctate fluorescence progrediently enlarged with increase of age (Figs 4B and 5), indicating an absolute increase of vitamin A. Using this parameter, linear correlations were found with liver tissue concentrations of retinoids (Fig. 6). Moreover, duration of ultraviolet epi-illumination necessary for complete disappearance of fluorescent spots increased from 3.1 ± 0.1 s to 5.2 ± 0.3 s, 12.1 ± 1.4 s and 20.1 ± 0.1 s in livers with the age of 1, 3, 12 and 24 months and was

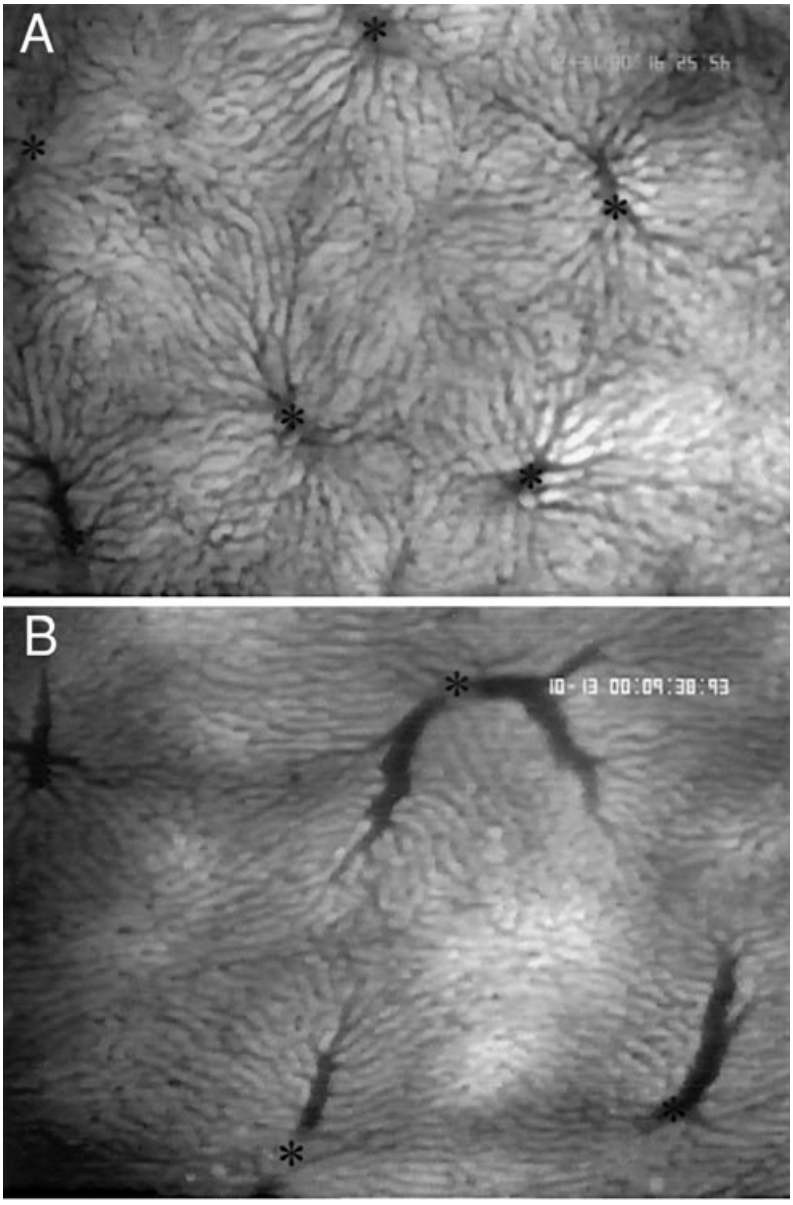

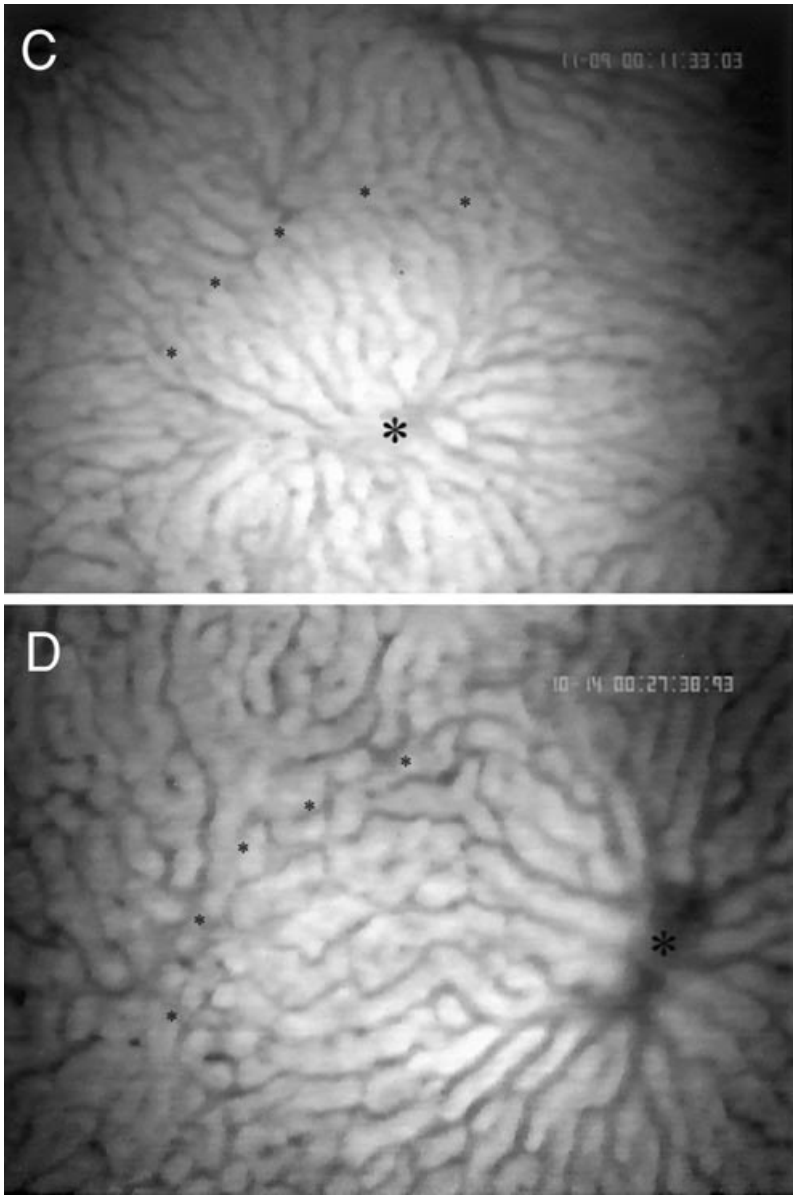

Fig. 3. Representative intravital fluorescence microscopic images of livers at the age of 1 month (A and C) and 24 months (B and D) after contrast enhancement by intravenously applied sodium fluorescein. Note the growth/enlargement of individual lobules which are indicated by their central draining postsinusoidal venules (asterisks) as well as the concomitant increase of postsinusoidal venules in length and diameter from neonate (1 month, A) to senescent age (24 months, B). High magnification of individual lobules clearly displays the increase of length from the periportal (small asterisks) to the pericentral area (single large asterisk) during ageing of livers from 1 month (C) to 24 months (D). Blue-light epi-illumination technique, magnification × 100 (A and B), magnification × 200 (C and D).

found to correlate with both the retinoids ($r^2 > 0.9$) and the microscopically assessed area of vitamin A autofluorescence ($r^2 = 0.913$).

By intra-arterial injection of fluorescent latex particles, the quantitative analysis of their clearance kinetics revealed comparable phagocytic activity of Kupffer cells in animals of different age (Fig. 7A). Moreover, the intralobular distribution of latex particles did not differ between the different age groups (Fig. 7B).

Intrahepatic leucocyte–endothelial cell interaction

The average number of leucocytes passing the liver within a certain time period, i.e. the leucocyte flux through sinusoids and postsinusoidal venules was found 2 to 2.5 fold higher in the 3- and 12 month-old-animals when compared to animals of one month of age (Table 4). Detailed analysis of leucocyte flow behaviour, however, indicated that most of the leucocytes passing the liver did not interact

Table 2. Lobular liver architecture and sinusoidal microhemodynamics in rats at the age of 1, 3, 12, and 24 months, as assessed by *in vivo* fluorescence microscopy with an epi-illumination technique

	1 month	3 month	12 month	24 month
Postsinusoidal venules				
-Length (μm)	218 ± 13#	280 ± 26+	349 ± 15	445 ± 50
-Diameter (μm)	21 ± 1#	30 ± 2+	37 ± 1+	49 ± 3
-Vascular space (μm²)	4637 ± 592#	9796 ± 1706+	14865 ± 828+	23243 ± 3072
Sinusoidal density (n/200 μm)	8.6 ± 0.3+	7.9 ± 0.2	7.8 ± 0.1	7.5 ± 0.2
Sinusoidal perfusion rate (%)	98.8 ± 0.6	8.0 ± 1.5	99.6 ± 0.3	98.4 ± 0.5
Sinusoidal diameter (μm)	5.56 ± 0.15*	6.70 ± 0.16	6.66 ± 0.17	6.66 ± 0.12
Sinusoidal blood flow velocity (μms)	315 ± 9#	261 ± 23	222 ± 24	196 ± 22
Sinusoidal blood flow (pL/s)	7.7 ± 0.5	9.3 ± 0.7	7.8 ± 0.8	6.8 ± 0.7

All values are given as mean ± SEM, each group = 6* $P < 0.05$ versus 3, 12 and 24 months; # $P < 0.05$ versus 12 and 24 months; + $P < 0.05$ versus 24 months.

Table 3. Concentrations of retinol and retinyl esters in total liver homogenates of rats at the age of 1, 3, 12, and 24 months, as assessed by high pressure liquid chromatography

	1 month	3 month	12 month	24 month
Retinol (μg/g liver)	42 ± 15+	55 ± 3	64 ± 15	73 ± 7
Retinyl stearate (μg/g liver)	7 ± 0 *	84 ± 18#	192 ± 12	222 ± 28
Retinyl palmitate (μg/g liver)	60 ± 1 *	878 ± 161#	2909 ± 268	3167 ± 321
Retinyl oleate (μg/g liver)	2 ± 0 *	35 ± 7#	79 ± 4	131 ± 20

All values are given as mean ± SEM, each group $n = 6$. *$P < 0.05$ versus 3, 12 and 24 months; # $P < 0.05$ versus 12 and 24 months; + $P < 0.05$ versus 24 months.

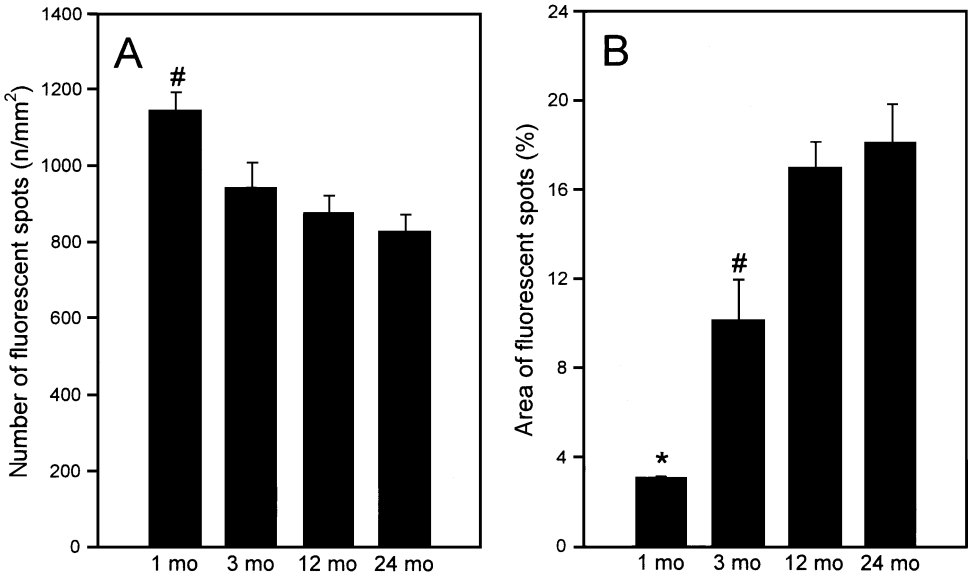

Fig. 4. Number of fluorescent spots (A), given per mm² observation area, and area of fluorescent spots (B), given in percentage of the observation area, as assessed by *in vivo* fluorescence microscopy and ultraviolet epi-illumination in livers of rats at the age of 1 month ($n = 6$), 3 months ($n = 6$), 12 months ($n = 6$) and 24 months ($n = 6$). Mean ± SEM. * $P < 0.05$ versus 3, 12 and 24 months; # $P < 0.05$ versus 12 and 24 months.

with the hepatic microvascular endothelium. The percentage of leucocytes exhibiting loose contact by rolling along the microvascular endothelium of postsinusoidal venules ranged between 17% and 24% (Table 4). The number of leucocytes, which were found stagnant within sinusoids or adherent in postsinusoidal venules were less than 20 cells/lobule and 150 cells/mm² endothelial surface, indicating physiological values (Table 4).

Hepatic bile flow and serum liver enzyme activities

Bile flow serving as a parameter of hepatocellular excretory function was found highest in the weanling rats and subsequently decreased to ~45–50% at the age of 12 and 24 months (Table 5).

Reflecting osteogenesis, arterial blood samples revealed higher activities of alkaline phosphatase in young (3 month), but in particular in

Table 4. Leukocyte flow behaviour and leucocyte–endothelial cell interaction in livers of rats at the age of 1, 3, 12, and 24 months, as assessed by *in vivo* fluorescence microscopy with an epi-illumination technique

	1 month	3 month	12 month	24 month
Sinusoids				
-Leucocyte flux (n/min)	47 ± 13 $^{\$}$	128 ± 16^{+}	99 ± 6 $^{+}$	57 ± 5
-Leucocyte stasis (n/lobule)	8 ± 3	17 ± 3 $^{+}$	8 ± 2	5 ± 1
Postsinusoidal venules				
-Leucocyte flux (n/min)	25 ± 5	92 ± 15	72 ± 4	60 ± 11
-Leucocyte rolling (%)	17 ± 6	19 ± 3	19 ± 1	24 ± 1
-Leucocyte adherence (n/mm^2)	52 ± 13	145 ± 32	128 ± 18	94 ± 24

All values are given as mean ± SEM, each group $n = 6$. $^{\$}$ $P < 0.05$ versus 3 and 12 months; $^{+}P < 0.05$ versus 24 months.

Table 5. Bile flow and liver enzyme activities in serum of rats at the age of 1, 3, 12, and 24 months

	1 month	3 month	12 month	24 month
Bile flow (µl/g liver x 20 min)	34.4 ± 7.7$^{\$}$	26.9 ± 3.4	15.7 ± 1.7	19.5 ± 2.4
Alkaline phosphatase (U/l)	337 ± 51*	177 ± 25	73 ± 5	93 ± 12
Aspartate aminotransferase (U/l)	134 ± 14	146 ± 13	65 ± 10	114 ± 21
Alanine aminotransferase (U/l)	36 ± 4	40 ± 3	85 ± 32	78 ± 14
Glutamate dehydrogenase (U/l)	31 ± 11	30 ± 7	19 ± 3	23 ± 5

All values are given as mean ± SEM, each group $n = 6$. *$P < 0.05$ versus 3, 12 and 24 months; $^{\$}$ $P < 0.05$ versus 12 months.

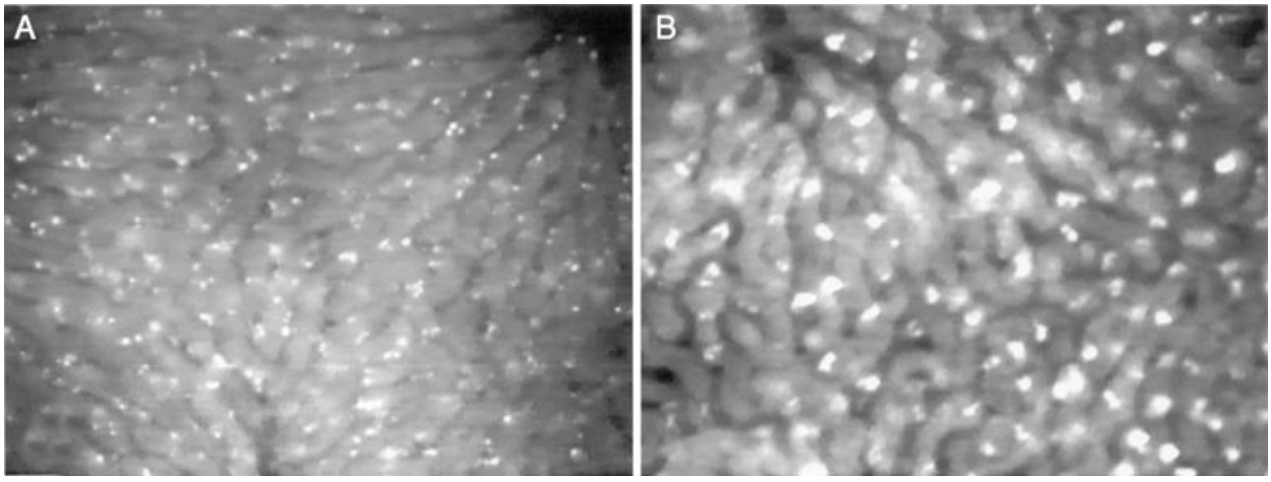

Fig. 5. Representative intravital fluorescence microscopic images of livers at the age of 1 month (A) and 24 months (B) upon ultraviolet epi-illumination. Note the hepatic stellate cell-associated small-sized autofluorescent spots of stored vitamin A at the age of 1 month (A) when compared to the increased size of hepatic stellate cell-associated area of vitamin A autofluorescence at the age of 24 months (B). Magnification × 200.

neonate/weanling rats (1 month) when compared to the 12 month and 24 month-old-animals. Physiological serum activities of aspartate aminotransferase, alanine aminotransferase and glutamate dehydrogenase in animals of either age indicate absence of hepatocellular disintegration (Table 5).

Discussion

Two criteria have been of particular importance for us in selecting Sprague–Dawley rats for the present study: first, in the past intravital fluorescence microscopy of the rat liver allowed significant advances in our understanding of the physiology and pathophysiology of hepatic microcirculation; however, this has not been extensively applied to assess age-related changes. Secondly, the majority of gerontological investigations are done in rats. However, extrapolation from the present data to another species should be drawn with caution, because already within a species different strains might give divergent results (22). Moreover, since several parameters of the aged liver, such as liver size, differ between rats and humans, extrapolation to the human situation

might be impossible. Nonetheless, the present information on Sprague–Dawley rats, which are one of the most common strain/stock of rats used in animal research, should prove useful in helping to understand the influence of age on liver physiology.

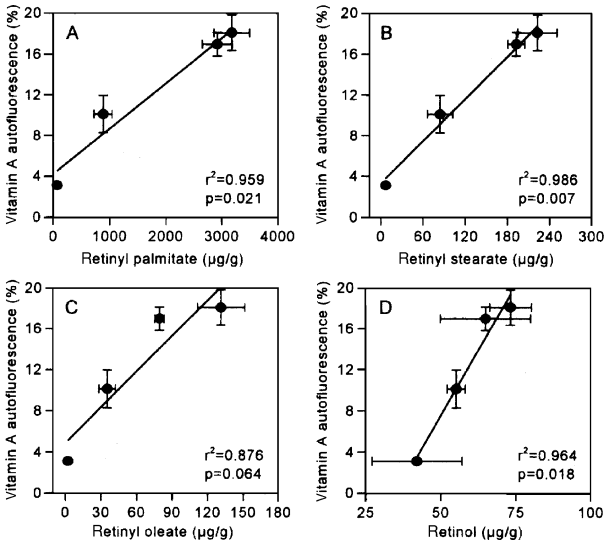

Fig. 6. Regression analysis between hepatic tissue concentrations (µg/g) of retinyl palmitate (A), retinyl stearate (B), retinyl oleate (C), and retinol (D) and the *in vivo* fluorescence microscopically assessed size of vitamin A autofluorescence (in percentage of the observation area) in livers of rats at the age of 1 month ($n = 6$), 3 months ($n = 6$), 12 months ($n = 6$) and 24 months ($n = 6$). Mean ± SEM. r, regression coefficient.

As vitamin A storing hepatic stellate cells are the key effector in hepatic fibrogenesis (23), the accurate on-line *in vivo* documentation of sites of vitamin A autofluorescence is of pivotal interest for research in liver pathology. In the present study, we provide an accurate *in vivo* measure of vitamin A autofluorescence by analysing number and area of the fluorescent sites. With increase of age of the liver studied, the simple assessment of the number of fluorescent spots revealed a fictitious reduction of the number of hepatic stellate cells. However, with the age-dependent accumulation of vitamin A, single fluorescent spots increase in size and overlap with the consequence of loss of individual cell discrimination. Consideration of size of fluorescence, as presented here, properly reflects the vitamin A storage per tissue unit. This is strongly underlined in the present study by the significant correlations using regression analysis between the areas of vitamin A autofluorescence and chromatographically assessed tissue concentrations of retinoids.

Sprague–Dawley rats of various age exhibited changes of systemic haemodynamics, i.e. the age-dependent increase of systemic blood pressure and decrease in heart rate, similarly as commonly observed in humans. Global parameters, such as body weight as well as absolute and relative liver weight have also been shown as a function of age and are in accordance with previously published data in rats (22). The tendency in loss

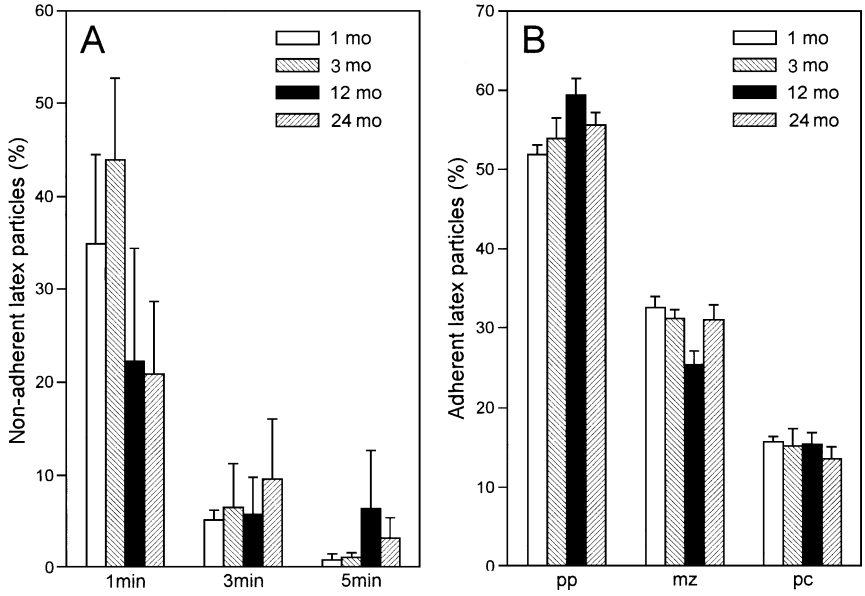

Fig. 7. Kinetics of adherence of latex particles (A), i.e. the number of non-adherent fluorescent labelled latex particles at 1, 3 and 5min after intra-arterial injection, given as percentage of all particles visible in microscopic fields observed for 10 s assessed by means of *in vivo* fluorescence microscopy. (B) displays the distribution of adherent latex particles (as percentage of all particles visible per observation field) in the periportal (pp), midzonal (mz) and pericentral (pc) segments of sinusoids. *In vivo* fluorescence microscopic measurements were performed in livers of rats at the age of 1 month ($n = 6$), 3 months ($n = 6$), 12 months ($n = 6$) and 24 months ($n = 6$). Mean ± SEM.

of body weight, as ageing progressed to senescent stages, might best be interpreted by whole body protein catabolism, frequently occurring with high age (24).

The present experiments show that neither during maturation nor during ageing and senescence significant remodelling of the liver occurs. The liver increases in mass during the period from weanling to late juvenile and adult life; however, relative liver weight was highest at the age of one month with a liver-to-body weight ratio of ~3.8%, and decreased to values ranging between 2.4% and 2.9% during the subsequent life-span. From 1 month up to 12 months of age, the 2.9-fold increase in liver mass was paralleled by a 3.5-fold increase of the average size of intrahepatic lobules. The present results are in line with a previous study, demonstrating an increase of acinar diameter from weanling (50–70 g) to juvenile rats (~300 g) (25), but extend the information in that the size of hepatic lobules increase until adulthood without further changes during senescence. This implies that the age-related adaptation of hepatic morphology to enlarged tissue is not an increase of the absolute number of lobules, but merely the growth of previously existing morphological units. Thereby, intrahepatic lobules maintained their hexagonal structure with blood originating from afferent microvessels and drained through the periportal, midzonal and percentral regions of the sinusoids into the central postsinusoidal venules. The latter passively adapted to lobular enlargement by their proportional increase of length and diameter to meet the organ's longitudinal and transverse growth, as this has similarly been described for arterioles and venules of intestinal (26) and cutaneous tissue (27) during maturational ageing to adulthood. In parallel, sinusoids revealed a significant increase in diameter between weanling animals and those of 3, 12, or 24 months of age with a concomitant decrease in sinusoidal blood flow velocity from immature to mature and old aged animals, similarly as this was described by Drugas et al. (25).

In the light of unchanged numbers of sinusoids during the whole lifespan, the microvessels would be spread apart from each other as hepatic tissue enlarges with age. Thus, one might expect a reduction in sinusoidal density, which inversely correlates with the 3.5–4-fold increase of lobular size. However, sinusoidal density was found only moderately reduced to 87%, which provides strong evidence for recruitment and/or new formation of sinusoidal microvessels, for the maintenance of adequate oxygen supply despite the increase in tissue mass.

An important result of the present study is the fact that in the absence of stress the ability of Kupffer cells to phagocytize does not differ between animals of different age, as indicated by comparable kinetics of clearance of circulating latex particles. Thus, observations that aged rats were more susceptible to endotoxin- (11) or cadmium-induced hepatic injury (10) compared to young rats, have to be explained by altered properties and limited capabilities of aged Kupffer cells to deal with stress factors and to mount proper stress responses, rather than by phagocytic dysfunction *per se*. In line with this view, it has been postulated that the age-associated decrease of the senescent marker protein-30 may induce deregulation of Ca^{2+}-homeostasis and alteration of the signalling system in aged tissue with improper responses and increased susceptibility to various harmful stimuli (28, 29). Moreover, the age-associated increase of the basal levels of proinflammatory cytokine IL-1β and decrease of basal levels of anti-inflammatory IL-6 might cause aged rats more prone to hepatotoxic events (8), while intrahepatic leucocyte–endothelial cell interaction, which was found within the physiological range in all animals regardless their age, seems not to primarily reflect the age-associated sensitivity to injury.

In summary, the data provided here offer expanded and detailed information on liver morphology, microangioarchitecture and intrahepatic cellularity in male Sprague–Dawley rats of various ages. Consideration and incorporation of age-specific parameters will help in understanding the influence of age on physiological and pathophysiological events.

Acknowledgements

This study is supported by a grant from the Deutsche Forschungsgemeinschaft (Vo 450/5–1 and 5–2). B.V. is recipient of a Heisenberg Stipendium of the Deutsche Forschungsgemeinschaft, Bonn-Bad Godesberg, Germany (Vo 450/6–1 and 6–2). The authors thank Ruth Nickels for excellent assistance in HPLC analysis.

References

1. Rikans L E. Influence of aging on the susceptibility of rats to hepatotoxic injury. Toxicol Appl Pharmacol 1984; 73: 243–9.
2. Woodhouse K W, Mutch E, Williams F M. The effect of age on pathways of drug metabolism in human liver. Age Ageing 1984; 13: 328–4.
3. Woodhouse K W. Drug handling by the ageing liver: past work and future directions. Rev Clin Gerontol 1996; 6: 215–23.
4. Klinger W. Biotransformation of drugs and other xenobiotics during postnatal development. Exp Toxicol Pathol 1996; 48: 1–88.

5. George G, Wynne H A, Woodhouse K W. The association of age with the induction of drug-metabolizing enzymes in human monocytes. Age Ageing 1990; 19: 364–7.
6. Woodhouse K W, James O F. Hepatic drug metabolism and ageing. Br Med Bull 1990; 46: 22–35.
7. Wynne H A, Goudevenos J, Rawlins M D, et al. Hepatic drug clearance: the effect of age using indocyanine green as a model compound. Br J Clin Pharmacol 1990; 30: 634–7.
8. Rikans L E, Decicco L A, Hornbrook K R, Yamano T. Effect of age and carbon tetrachloride on cytokine concentrations in rat liver. Mech Ageing Dev 1999; 108: 173–82.
9. Sanz N, Diez-Fernandez C, Alvarez A M, et al. Age-related changes on parameters of experimentally-induced liver injury and regeneration. Tox Appl Pharmacol 1999; 154: 40–9.
10. Yamano T, Shimizu M, Noda T. Age-related change in cadmium-induced hepatotoxicity in Wistar rats. Role of Kupffer cells and neutrophils. J Appl Pharmacol 1998; 151: 9–15.
11. Durham S K, Brouwer A, Barelds R J, et al. Comparative endotoxin-induced hepatic injury in young and aged rats. J Pathol 1990; 162: 341–9.
12. Hendriks H F J, Horan M A, Durham S K, et al. Endotoxin-induced liver injury in aged and subacutely hypervitaminotic rats. Mech Ageing Dev 1987; 41: 241–50.
13. Baker H J, Lindsey R J, Weisbroth S H. The Laboratory Rat. 1979. Academic Press Inc New York, Vol. 1: 411.
14. Vollmar B, Glasz J, Leiderer R, et al. Hepatic microcirculatory perfusion failure is a determinant of liver dysfunction in warm ischemia-reperfusion. Am J Pathol 1994; 145: 1421–31.
15. Vollmar B, Menger M D, Glasz J, et al. Impact of leukocyte–endothelial cell interaction in hepatic ischemia-reperfusion injury. Am J Physiol 1994; 267: G786–93.
16. Vollmar B, Glasz J, Post S, Menger M D. Depressed phagocytic activity of Kupffer cells after warm ischemia-reperfusion of the liver. J Hepatol 1994; 20: 301–4.
17. Vollmar B, Rüttinger D, Wanner G A, et al. Modulation of Kupffer cell activity by gadolinium chloride in endotoxemic rats. Shock 1996; 6: 434–41.
18. Zeintl H, Tompkins W R, Messmer K, Intaglietta M. Static and dynamic microcirculatory video image analysis applied to clinical investigations. Prog Appl Microcirc 1986; 11: 1–10.
19. Vollmar B, Siegmund S, Menger M D. An intravital fluorescence microscopic study of hepatic microvascular and cellular derangements in developing cirrhosis in rats. Hepatology 1998; 27: 1544–53.
20. Gross J F, Aroesty J. Mathematical models of capillary flow. A critical review. Biorheology 1972; 9: 225–64.
21. Rappaport A M. The microcirculatory hepatic unit. Microvasc Res 1973; 6: 212–28.
22. Schoeffner D J. Warren D A, Muralidhara S, Bruckner J V. Organ weights and fat volume in rats as a function of strain and age. J Toxicol Environ Health 1999; 56: 449–62.
23. Friedman S L. Cytokines and fibrogenesis. Semin Liver Dis 1999; 19: 129–40.
24. Blechman M B, Gelb A M. Aging and gastrointestinal physiology. Clin Geriatric Med 1999; 15: 429–38.
25. Drugas G T, Chun K E, Miescher E A, Clemens M G. Maturational differences in hepatic microhemodynamics in rats. J Surg Res 1993; 54: 246–53.
26. Unthank J L, Bohlen H G. Quantification of intestinal microvascular growth during maturation: techniques and observations. Circ Res 1987; 61: 616–24.
27. Vollmar B, Morgenthaler M, Amon M, Menger M D. Skin microvascular adaptations during maturation and aging of hairless mice. Am J Physiol 2000; 279: H1591–9.
28. Fujita T. Senescence marker protein-30 (SMP-30): Structure and biological function. Biochem Biophys Res Comm 1999; 254: 1–4.
29. Fujita T, Shirasawa T, Maruyama N. Expression and structure of senescence marker protein-30 (SMP30) and its biological significance. Mech Ageing Dev 1999; 107: 271–80.